scientific reports

Check for updates

OPEN

Origin of the high coercivity in FeNi inspired magnets

A. Hernando[1,4,6,8], P. de la Presa[4,5], J. A. Jiménez-Rodríguez[3], A. García-Escorial[3], D. Arranz-López[4], J. Calvo[7], P. Marín[4,5], I. Llamas[1], C. Navío[1] & R. Miranda[1,2]✉

In samples taken from iron meteorites, the presence of the nanocrystallites of FeNi with a $L1_0$ crystalline structure embedded in a complex matrix produces a magnetic behavior of the whole sample characterized by large magnetization at saturation and large coercive field. This has created expectations to obtain strong magnets without rare earths based on the $L1_0$ FeNi phase. In artificially synthetized samples containing several phases, the presence of the $L1_0$ phase was often deduced from the observation of coercive fields of several hundreds of Oe. Here, the microstructure and the magnetic behavior of crystallized microwires cast from Fe, Ni and P has been thoroughly analyzed. Microwires containing only two phases: plate-shaped, single-domain, nanocrystallites of the soft fcc (A1) FeNi phase embedded in a schreibersite $(Fe_xNi_{1-x})_3P$ matrix show large room temperature coercivities of 440 Oe, which decrease substantially by cooling the sample below the Curie temperature of the matrix. It is shown experimentally that such behavior indicates that the origin of the high coercivity is the microstructure that isolates magnetically the crystallites of the soft FeNi A1 phase. The results point out that the presence or absence of $L1_0$-FeNi ordered phase is irrelevant in first order to achieve coercivity of hundreds of Oe in these types of alloys. In fact, it is the combination of microstructure and shape anisotropy that causes the high coercivity.

Permanent magnets are a crucial part of modern society, due to the increasing electrification of daily life. Since their discovery, rare-earth-based permanent magnets have dominated the market. This has made rare earths a critical resource of high geopolitical importance. The production of rare earths, however, is highly polluting, and therefore, the development of novel rare-earth-free, hard magnetic materials has become of strategic importance. The discovery in iron meteorites of nanocrystallites of a presumably hard magnet consisting only in Fe and Ni, in the equiatomic, chemically ordered fct $L1_0$ phase, arose considerable interest[1–10]. The existence of this hard magnetic FeNi phase (tetrataenite) is most intriguing since the equiatomic FeNi alloy also presents the well-known, chemically disordered and magnetically soft, fcc (A1) FeNi phase. The difference between the two phases is given by the random occupation of the atomic sites in the fcc lattice by Fe and Ni for the A1 phase or the chemical ordering of Fe and Ni in alternating planes along the crystallographic c axis present in the $L1_0$ phase[3,7]. This chemical ordering results in large magnetocrystaline uniaxial anisotropy (0.2–1.3 MJ/m^3)[3,5,8,9], and a large theoretical maximum magnetic energy product, $(BH)_{max} \approx 42$ MG·Oe[4]. The chemical order is stable up to 320 °C, beyond which it starts to disorder, forming the A1 FeNi phase and losing its magnetic anisotropy[10].

In nature, the ordered $L1_0$ phase has only been observed as nanocrystallites (10–150 nm) embedded in another phases (often complex FeNi phosphides) in meteorites, where it is formed over millions of years under extremely slow cooling rates, ranging from 0.1 to 100 °C per million years[1–7]. Samples extracted from meteorites, where the nanocrystallites of the $L1_0$ phase are embedded in complex matrices, display coercive fields in the range 500 - 1000 Oe. Some studies on samples taken from meteorites [6] suggest that for best hard magnetic performance, tetrataenite regions should be small enough to be single domain, which is ≈ 45 nm for $L1_0$ FeNi [1].

The artificial synthesis of the bulk form of the $L1_0$ FeNi phase is challenging due to its low order–disorder temperature. Atomic mobility is extremely slow at temperatures where the ordered phase is stable, and nowadays, there is no established method for synthesizing bulk samples with a high $L1_0$ phase content, although a wide range of techniques have been explored. They include amorphous precursor crystallization[11–18], defect engineering and pressure methods[19], oxidation–reduction cycles[20,21], nitrogen insertion and topographic extraction (NITE)[22,23], and electrodeposition[24]. While it has been claimed that $L1_0$ FeNi has been successfully synthetized with most of these techniques, a careful reading of the publications reveals that the $L1_0$ phase content remains minimal, and,

[1]IMDEA Nanociencia, 28049 Madrid, Spain. [2]Departamento de Física de La Materia Condensada, Universidad Autónoma de Madrid, 28049 Madrid, Spain. [3]CENIM, CSIC, 28040 Madrid, Spain. [4]Instituto de Magnetismo Aplicado, 28230 Madrid, Spain. [5]Departamento de Física de Materiales, Universidad Complutense de Madrid, 28040 Madrid, Spain. [6]Donostia International Physics Center, 20018 San Sebastián, Spain. [7]Micromag 2000 S. L., 28925 Arroyomolinos, Alcorcón, Madrid, Spain. [8]Universidad Antonio de Nebrija, 28015 Madrid, Spain. ✉email: rodolfo.miranda@imdea.org

often, even doubtful. Some techniques, such amorphous precursor crystallization, have yielded coercivities of hundreds of Oe, much higher than expected for samples predominantly composed of a soft magnetic phase[11–17]. These enhanced magnetic properties are typically attributed to an increase of the percentage of the $L1_0$ phase of the samples, neglecting the effect of the microstructure in the coercivity.

Coercivity, however, being an extrinsic magnetic property is controlled by the microstructure of the samples. Here we focus on the effect of the microstructure on the magnetic properties of nanocrystalline microwires obtained by cooling at the adequate rate FeNiP master alloys, in which the only present ferromagnetic phase is the soft A1 FeNi phase. We demonstrate that samples with the right microstructure show high (440 Oe) values of coercivity at 300 K, similar to many of the samples previously reported to contain traces of the $L1_0$ FeNi phase. This relatively high coercivity is rather due to the shape anisotropy of FeNi fcc single-domain nanocrystals embedded in a paramagnetic tetragonal $(Fe_xNi_{1-x})_3P$ matrix, which magnetically isolates them.

Results

The Fe, Ni and P master alloys (MA) prepared by melting the corresponding powders consist of only two crystalline phases: a tetragonal, non-centrosymmetric schreibersite $(Fe_{1-x}Ni_x)_3P$ phase with lattice parameters $a = 8.97$ Å, and $c = 4.4$ Å and an fcc FeNi metallic phase (A1) with a lattice constant of 3.58 Å. Magnetic measurements indicate that the master alloys at 300 K are magnetically soft ($H_c = 20$ Oe), with saturation magnetizations of 56–62 emu/g, corresponding to the spontaneous magnetization of fcc FeNi and that the $(Fe_{1-x}Ni_x)_3P$ phase is paramagnetic above 190 K. Details of the preparation and characterization of the master alloys are given in the Supplementary information.

From these master alloys, Fe–Ni-P microwires (Mws) are prepared by casting with ejection speeds between 50 and 500 m/min. Up to 200 m/min, the microwires (Mw) are nanocrystalline, while above 200 m/min, the Mws are amorphous.

The microwire 21 was obtained at ejection speed of 50 m/min. The difference between the experimental (blue dots) and the fitted simulated (red line) patterns is plotted as a continuous black line. Only two phases appear in the fit: fcc γ-FeNi (green) and schreibersite $(Fe1\text{-}xNix)_3P$ (orange). The quality of the fit is numerically quantified by the corresponding figures of merit: the weighted profile residual of the least squares fit, R_{wp}, the statistically expected profile residual, R_{exp}, and the goodness of fit (sometimes referred as chi-squared), GoF.

Figure 1 shows the X-Ray diffraction pattern of a representative microwire (Mw21) obtained from the Fe–Ni master alloy with ejection speed of 50 m/min together with the Rietveld refined fit, which shows that the full diffractogram can be fitted with only the same two phases that appear in the master alloy, namely a mixture of A1 FeNi and $(Fe_{1-x}Ni_x)_3P$. As summarized in Table 1, the fcc, A1 phase is characterized by an average crystallite size of 22 nm and a = 3.58 Å, while the $(Fe_{1-x}Ni_x)_3P$ phase has crystallite size of 52 nm and lattice parameters c = 9.01 and a = 4.44 Å, respectively.

All nanocrystalline Mws produced showed the presence of the same two phases: $(Fe_{1-x}Ni_x)_3P$ with S_4 symmetry and fcc A1 FeNi, with lattice constants similar to those observed in the master alloy and weight percentages ranging from 63.5% to 84.5% for $(Fe,Ni)_3P$ and from 36.5% to 15.5% for A1 FeNi , respectively. The average crystallite size of the fcc FeNi phase in the different microwires ranges from 8 to 28 nm. It must be noted that the domain wall thickness for pure Fe is 20 nm and should be much larger (≈ 400 nm) for FeNi alloys with its small anisotropy constant[11]. Consequently, the grain size of the cubic phase indicates that the crystallites are magnetically single-domain.

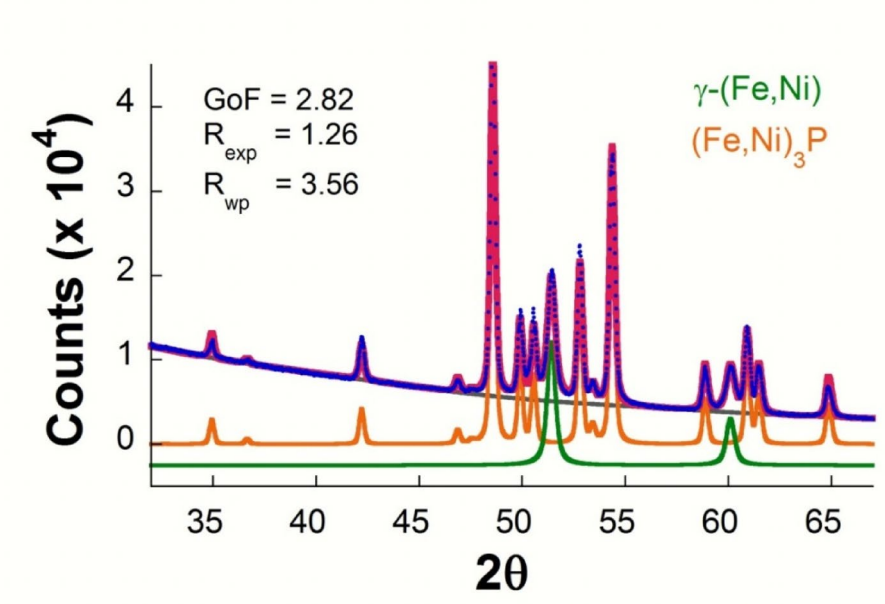

Fig. 1. Experimental XRD pattern and Rietveld refinements of a as-casted representative microwire.

Phase	Space group	Percentage	Lattice parameters (nm)	Crystallite size (nm)
(Fe,Ni)3P	$I\bar{4}$	74.9%	a = 0.9014 c = 0.4446	52
(A1) γ-(Fe,Ni)	$Fm\bar{3}m$	25.1%	a = 0.3579	22

Table 1. Microstructural parameters obtained from the Rietveld refinement of the diffraction patterns of the representative microwire Mw-21.

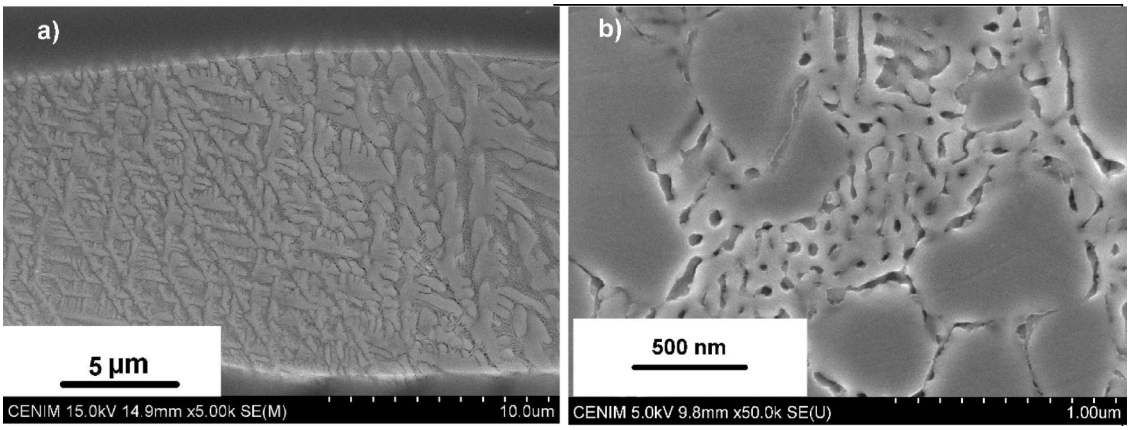

Fig. 2. Observations by electron microscopy SEM-micrographs of as-cast Mw-21 recorded in a section parallel to the axis of the wire showing (**a**) primary columnar dendrites of $(Ni,Fe)_3P$ and (**b**) interdendritic nano-sized lamellae of $(Ni,Fe)_3P$ and A1 FeNi formed during the eutectic reaction. The microstructure present in the cross-sections was also observed, but it did not provide any additional relevant information.

The presence of $L1_0$ FeNi phase above the detection limit of present XRD set up (0.12%) cannot be confirmed in any of the microwires. It has been reported that the addition of phosphorus to Ni alloys does increase atomic diffusivities[25], allowing the plane-by-plane atomic ordering in A1 FeNi to achieve the formation of $L1_0$ tetrataenite in timescales practicable for production of magnets. However, the results of the measurements performed in the conventionally cast samples showed that the presence of phosphorus is *not* sufficient to induce a detectable $L1_0$-type ordering in this phase. Laboratory-based XRD can be used to confirm the presence of an $L1_0$ type of order in the fcc A1 FeNi phase. The relative intensity of the superlattice [100] peak of the $L1_0$ phase with respect to the most intense fundamental [200] reflection peak for a bulk FeNi sample has been calculated for the photon energy used (Cu Kα, λ = 1.5406 Å) to be 5.8×10^{-2}, i.e. within the detection limits of XRD.

The X-ray diffraction patterns recorded for the microwires did not show preferred crystallographic orientation in the microstructure, which was also examined by SEM. Figure 2 reproduces images of the representative, as-casted Mw21. Figure 2a shows primary columnar dendrites surrounded by irregular nano-sized lamellae of $(Fe_{1-x}Ni_x)_3P$ and A1 FeNi, typically 20 nm-wide with width/length ratios of 0.3–0.7, formed during the eutectic reaction (Fig. 2b). Measurements of the width and width/length ratio of the A1 FeNi phase within the interdendritic regions were performed using conventional quantitative metallographic techniques in SEM micrographs. The size of the lamellar structure resulting from the simultaneous precipitation of the solid phases $(Fe_{1-x}Ni_x)_3P$ and A1 FeNi during the eutectic reaction depends on the cooling rate. Therefore, the formation of nano-sized lamellae of A1 FeNi in the rapidly cooled samples will be responsible for the variations in the resulting magnetic behavior with respect to conventionally cast samples.

The isolation of the different lamellae of the A1-FeNi phase present in the interdendritic regions is a direct consequence of the process of eutectic solidification of the liquid. The (Fe,Ni)3P dendrites with tree-like structures form first from the main liquid, leaving behind a P-poor liquid in the interdendritic regions. When this remaining liquid reaches the eutectic composition, it will solidify at the specific eutectic temperature, forming a P-free phase (A1-FeNi) along with $(Fe,Ni)_3P$. Since the volume fraction of phase A1 is significantly less than that of $(Fe,Ni)_3P$, the fibrous structure observed in Fig. 2 is obtained, because the system can minimize its interfacial energy by selecting the morphology associated with the smallest interfacial area. Thus, as direct result of the eutectic reaction occurring in these specific locations, the A1-FeNi crystallites are isolated in the spaces between the solidified dendrite arms.

The Mws were obtained from the Fe–Ni master alloy and show coercive fields up to 440 Oe. The different values of the saturation magnetization (in emus) correlate with the radius of the microwires.

The magnetic properties of several nanocrystalline Mws obtained at ejection speeds below 100 m/min have been measured. All microwires exhibit room temperature coercive fields of the order of several hundreds of Oe, as shown in Fig. 3.

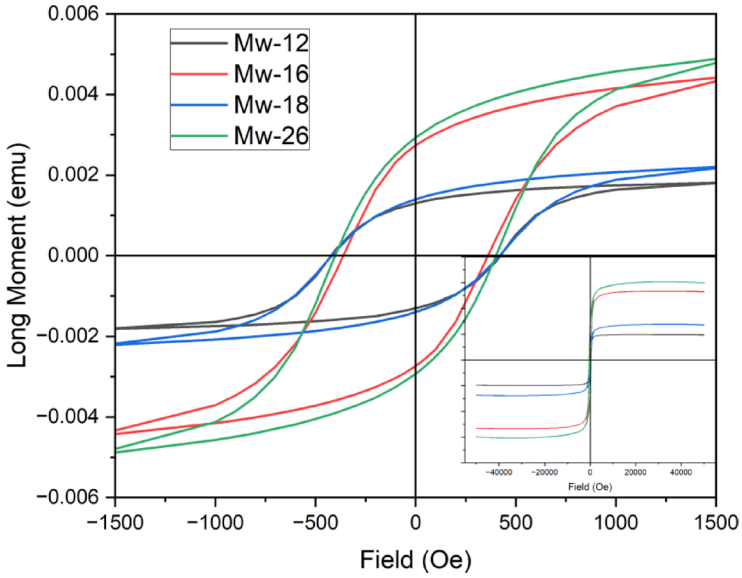

Fig. 3. Hysteresis cycles at 300 K for a number of nanocrystalline microwires.

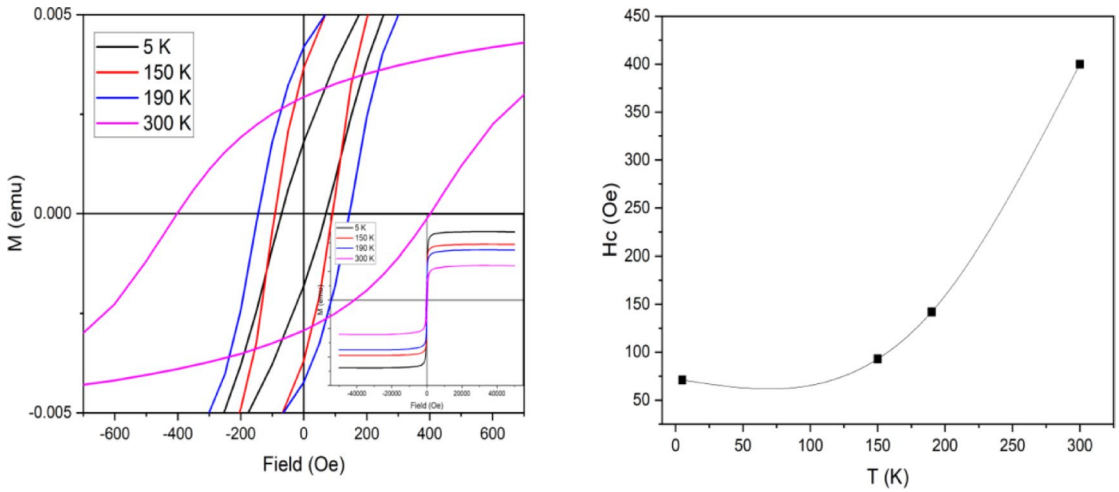

Fig. 4. Hysteresis cycles (left) and coercive field (right) as a function of temperature.

Figure 4 shows the thermal dependence of the hysteresis loop for the representative Mw-21. The increase of the coercive field with increasing T corresponds to an anomalous thermal dependence that is due to the ferromagnetic to paramagnetic transition of the matrix. In effect, as the temperature decreases approaching the Curie point of the $(Fe_{1-x}Ni_x)_3P$ phase at 190 K (see Supplementary information), the A1 FeNi crystallites start to be connected by exchange interactions through the (progressively magnetic) matrix and the coercivity strongly decreases. This anomalous thermal dependence of the coercivity has been also observed in different nanocrystalline samples consisting of ferromagnetic nanocrystals embedded in an amorphous soft ferromagnetic matrix[26,27], where a strong discontinuity in the coercivity occurs at the Curie temperature of the matrix, which is lower than the one of the nanocrystals. At 300 K the coercivity of microwire Mw-21 is of 400 Oe, similar to those observed for the other nanocrystalline microwires obtained from Fe–Ni master alloy, shown in Fig. 3.

The data corresponds to a representative microwire (Mw-21). A drastic decrease of coercivity with decreasing T is associated with the exchange coupling between A1 FeNi crystallites through the $(Fe_{1-x}Ni_x)_3P$ schreibersite matrix, which becomes ferromagnetic below 190 K.

Therefore, the magnetic character of the matrix determines the overall magnetic behavior of the system. If the matrix is a soft ferromagnet with Curie temperature T_m, below T_m, the single domains are coupled through the matrix inducing a soft collective behavior. At temperatures above T_m, the single domains become magnetically decoupled, and the coercive field undergoes a drastic increase.

In order to further demonstrate that a matrix that magnetically connects ferromagnetic crystallites results in a soft overall behavior of the sample, a new set of microwires has been casted from a master alloy MA-2

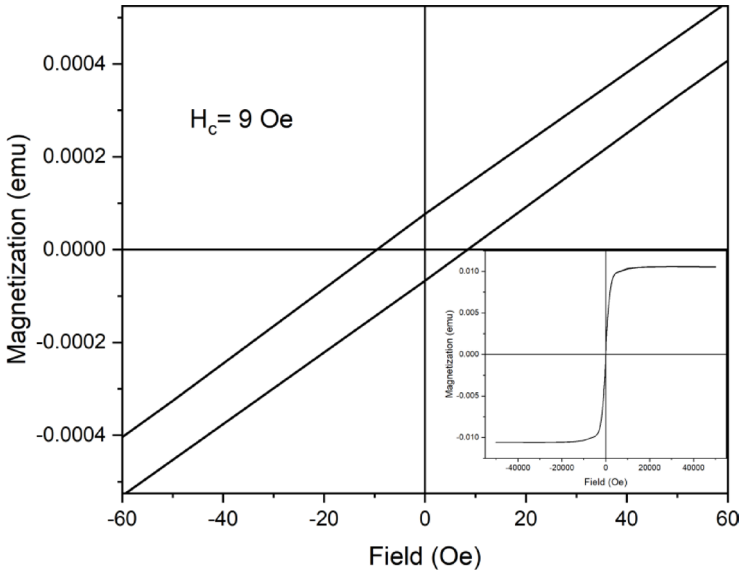

Fig. 5. Hysteresis cycle at 300 K for a microwire with bcc Fe crystallites coupled by a soft ferromagnetic matrix.

containing only Fe (see Methods section). In this case, the Mws contain bcc Fe crystallites with an average size of 22 nm, embedded in a matrix of soft Fe_3P schreibersite phase that is ferromagnetic at 300 K, its Curie temperature being 680 K[28]. Figure 5 shows that Mws obtained from a pure Fe master alloy, for which the room temperature ferromagnetism of Fe_3P schreibersite acts as exchange transmitter between the bcc cubic grains of Fe, exhibit low coercivity. This result illustrates the enormous influence exerted by the magnetic character of the matrix on the coercivity at room temperature of the crystalline microwires.

The microwire Mw-22, obtained from the master alloy MA-2 (without Ni). Notice the small coercivity produced by the bcc Fe_3P matrix being ferromagnetic at 300 K.

What causes the observed strength of the coercive field? The anisotropy constant of $Fe_{1-x}Ni_x$ alloys in the range of the Fe–Ni equi-atomic phase is of the order of 10^3 Jm^{-3} whereas that of Fe is 4×10^4 Jm^{-3}, with an associated anisotropy field of 570 Oe[25]. Therefore, a field of 420 Oe is too high to account for the coherent reversal of the FeNi single domain. On the other hand, 420 Oe is too small to be able of coherently reverse the magnetization in a single-domain of $L1_0$-FeNi phase in which the anisotropy constant is 32 times higher than in bcc Fe (corresponding anisotropy field of the order of 10^4 Oe). However, single crystals of the fcc Fe–Ni disordered phase can explain the observed coercivity after considering its lamellar structure achieved during eutectic phase segregation and observed in Fig. 2.

The difficulty to explain the observed values of coercivity from quantitative arguments based on crystalline anisotropy is eliminated when shape anisotropy is taken into account. The shape anisotropy field for a thin plate with a thickness t, and *h* and *w* corresponding to the larger and shorter dimensions of the plate (verifying $t<<w<h$) can be approximated as $H_{shape} = M_s\,(N_w - N_h)$ where $N_w = \frac{2t}{\pi w}$ and $N_h = \frac{2t}{\pi h}$[32]. According to the image shown in Fig. 2b, t lies in the cross section of the microwires. Let us write $h=\alpha t$ and $w=\beta t$ and the shape anisotropy field is given by $H_{shape} = \frac{2}{\pi\beta}M_s\left(1-\frac{\beta}{\alpha}\right)$. This field varies between 0, for a square platelet and $\frac{2}{\pi\beta}M_s$ for $\alpha>>\beta$. As $\frac{2}{\pi}M_s$ for $M_s = 130emu/g$ is of the order of 10^4 Oe, the anisotropy field should be of the order of 500 Oe when $\frac{1}{\beta}(1-\frac{\beta}{\alpha}) \cong 0.05$. This is a very reasonable average value for the actual nanometric platelets with widths, according to the XRD and electron microscopy data, of the order of 20 nm, and $\beta/\alpha \approx$ 0.3- 0.7, as observed in Fig. 2b.

Thus, the shape anisotropy could account for the coercivity observed in this work, and in previous ones reported for devitrified amorphous ribbons, provided that the plate-shaped single-domains are magnetically isolated to each other.

The magnetic hardening obtained during the microwire fabrication has been shown to be clearly associated with two facts: a) the drastic decrease of the crystalline size below the single domain size and b) the dispersion of these single-domains magnetically isolated by a non-ferromagnetic surrounding. The microstructure achieved by rapid cooling of the melt accomplishes the conditions required for reversal of magnetization by rotation, since the grain size is of the order of the single-domains and the grains are isolated at 300 K by the paramagnetic schreibersite phase. This is demonstrated by showing that the transit to ferromagnetism of this matrix phase gives rise to a drastic *decrease* of the coercivity. Therefore, the high coercivity of hundreds of Oe disappears as the matrix becomes ferromagnetic, allowing us to conclude that the intrinsic properties of the FeNi cubic phase are not only the determinant contributor to the coercivity. In several recent papers[12–18], the authors claimed that the presence of traces of chemically ordered $L1_0$-FeNi is the cause of coercivities of hundreds of Oe observed in

devitrified amorphous ribbons at 300 K. As demonstrated here, its presence, never clearly demonstrated, may not be needed for the observed large coercivity.

In conclusion, the influence of the microstructure in the high coercivity of rapidly solidified microwires with Fe, Ni and P content has been demonstrated in a simple system formed by only two well-defined crystalline phases. Values of coercivity of some hundreds of Oe are due to the presence of plate-shaped single domains of fcc FeNi embedded in a paramagnetic schreibersite matrix. When the matrix becomes ferromagnetic the coercivity falls down by an order of magnitude, thus showing an anomalous thermal dependence. The microstructure is spontaneously obtained by casting the wires from the melt and by the segregation of phases during cooling.

In samples taken from meteorites, the presence of the $L1_0$-FeNi phase in a matrix of the schreibersite phase has been reported to give rise to *average* magnetic properties, such as, large saturation magnetization ($M_s = 1270$ kA/m)[1], large uniaxial magnetic anisotropy energy ($K_u \approx 0.8–1.3$ MJ/m^3 and large coercive field ($H_c = 0.5$ kOe[5]-1.2 kOe[66]). Attempts to synthetize the phase by casting from amorphous precursors have used the observation of coercive fields of the order of several hundreds of Oe to demonstrate the presence of the phase. We demonstrate here that, given the microstructure of the samples produced by annealing, the presence of the $L1_0$ phase is not needed to produce coercivities in the range of 0.4 kOe. It is enough to have single-domain, platelet-shaped crystallites of the soft A1, fcc FeNi phase, magnetically isolated by a schreibersite matrix, paramagnetic at 300 K to determine the coercivity in first order.

Methods

The microwires have been obtained by melt-spinning the master alloys (MA) by the Taylor-Ulitovski procedure at different linear ejection speeds and, therefore, at different cooling rates. The ejection speed was swept between 500 and 50 m/min and was used as a parameter determining the cooling rate. The FeNiP master alloys were synthetized through melting highly pure Ni (99.99%) and/or Fe (99.9%) with a Fe_3P ferrophosphorus precursor.

The influence of water flux ejected on the melt as supplementary enhancement of the cooling rate has been used for further control. For ejection speed above 200 m/min, when applying the supplementary water flux, the microwires are amorphous, as derived from the XRD pattern. However, for ejection speeds between 200 and 50 turns per minute and without applying water flux the microwires are nanocrystalline and present the same two phases observed in the master alloy (see Supplementary Information).

Microstructural characterization of the samples was performed by the combined use of X-ray diffraction (XRD) and metallography observation with a scanning electron microscope (SEM). XRD was performed using Co radiation ($\lambda = 1.78897$ Å) in a Bruker D8 Discover equipped with an Eiger2R 250 K detector operated in continuous 1D mode with 33.8 mm (equatorial) and 20.6 mm (axial) opening. The XRD data were fitted by the Rietveld method using the version 4.2 of the analysis program TOPAS (Bruker AXS, GmbH, Karlsruhe, Germany) and a structural model containing the phases previously identified using the JCPDS data base, which crystallographic information was taken from the Pearson crystallographic database[29–31].

Magnetic characterizations have been performed in a SQUID magnetometer. Measurements of hysteresis loops were performed at 5, 150, 190 and 300 K. Magnetization as a function of temperature has been also measured from 5 to 300 K at 5000 Oe. For the magnetic characterization, 5 microwires of 10 mm each were used. The process of demagnetizing the coils has been carried out carefully for every measurement.

It must be noticed that a precise determination of the absolute value of the magnetization is difficult to obtain when measuring microwires due to the glass cover, as well as thickness fluctuations. However, the magnetization can be well measured in samples of master alloys. Since the crystalline phases of master alloys and microwires are the same, the experimental values obtained for the magnetization in master alloys can be assumed to be the same to those corresponding to microwires, assuming that evaporation during melting and casting of microwires may be neglected.

Data availability

The datasets used and/or analysed during the current study available from the corresponding author on reasonable request.

Received: 29 September 2025; Accepted: 19 January 2026
Published online: 22 January 2026

References

1. Albertsen, J. F., Aydin, M. & Knudsen, J. M. Mossbauer effect studies of taenite lamellae of an iron meteorite cape york. *Phys. Scr.* **17**, 467–472 (1978).
2. Clarke, R. S. Jr. & Scott, E. R. D. Tetrataenite—ordered FeNi, a new mineral in meteorites. *Amer. Mineral.* **65**, 624–630 (1980).
3. Albertsen, J. F. Tetragonal Lattice of Tetrataenite (Ordered Fe-Ni, 50–50) from 4 Meteorites. *Phys. Scr.* **23**, 301–306 (1981).
4. Lewis, L. H. et al. Inspired by nature: investigating tetrataenite for permanent magnet applications. *J. Phys. Condens. Matter* **26**(6), 064213 (2014).
5. Kotsugi, M. et al. Structural, magnetic and electronic state characterization of L10-type ordered FeNi alloy extracted from a natural meteorite. *J. Phys. Condens. Matter.* **26**, 064206 (2014).
6. Poirier, E. et al. Intrinsic magnetic properties of $L1_0$ FeNi obtained from meteorite NWA 6259. *J. Appl. Phys.* **117**, 17E318 (2015).
7. Nichols, C. I. O. et al. Variations in the magnetic properties of meteoritic cloudy zone. *Geochem. Geophys. Geosyst.* **21**(2), e2019GC008798 (2020).
8. Néel, L., Pauleve, J., Pauthenet, R., Laugier, J. & Dautreppe, D. Magnetic properties of an iron—nickel single crystal ordered by neutron bombardment. *J. Appl. Phys.* **35**, 873–876 (1964).
9. Woodgate, C. D., Patrick, C. E., Lewis, L. H. & Staunton, J. B. Revisiting Néel 60 years on: The magnetic anisotropy of L10 FeNi (tetrataenite). *J. Appl. Phys.* **134**, 163905 (2023).
10. Yang, C.-W. et al. A revision of the Fe-Ni phase diagram at low temperatures (<400 °C). *J. Phase Equilibr.* **17**, 522–531 (1996).

11. A magnetic single-domain particle should be small enough to not be able to sustain a domain wall in its interior. Thus, its size can be estimated as twice the length of a domain wall which is given by $\delta \approx \pi (A/K_u)^{1/2}$ where A is the exchange stiffness (related to the intensity of the exchange interaction) and K_u, the magnetic anisotropy. Introducing the values for $L1_0$ FeNi $K_u \approx 0.84–1.3$ MJ/m^3 and $A \approx 21 \times 10^{-12}$ J/m, $\delta \approx 22.6$ nm and the single domain characteristic size estimated for $L1_0$ FeNi would be ≈ 45 nm.
12. Makino, A. et al. Artificially produced rare-earth free cosmic magnet. *Sci. Rep.* **5**, 16627 (2015).
13. Sharma, P., Zhang, Y. & Makino, A. Magnetic properties of $L1_0$ FeNi phase developed through annealing of an amorphous alloy. *IEEE Trans. Magn.* **53**, 2100910 (2017).
14. Kim, J. et al. Properties of a rare earth free L10-FeNi hard magnet developed through annealing of FeNiPC amorphous ribbons. *Curr. Appl. Phys.* **19**, 599–605 (2019).
15. Hao, Z. et al. Effect of Si addition on the magnetic properties of FeNi-based alloys with $L1_0$ phase through annealing amorphous precursor. *J. Alloy. Compd.* **920**, 166029 (2022).
16. Wang, Y. et al. Formation of $L1_0$-FeNi hard magnetic material from FeNi-based amorphous alloys. *Chin. Phys. B* **31**, 046301 (2022).
17. Ivanov, Y. P. et al. Direct formation of hard-magnetic tetrataenite in bulk alloy castings. *Adv. Sci.* **10**, 2204315 (2023).
18. Houghton, O. S. et al. Reinterpretation of report of tetrataenite in bulk alloy castings. *Adv. Sci.* **12**, 2408796 (2024).
19. Tian, L.-Y. et al. Pressure effect on the order–disorder transformation in $L1_0$ FeNi. *Sci. Rep.* **10**, 14766 (2020).
20. Kurichenko, V. L., Karpenkov, D. Y., Karpenkov, A. Y., Lyakhova, M. B. & Khovaylo, V. V. Synthesis of FeNi tetrataenite phase by means of chemical precipitation. *J. Magn. Magn. Mater.* **470**, 33 (2019).
21. Lima, E., Drago, V., Fichtner, P. F. P. & Domingues, P. H. P. Tetrataenite and other Fe–Ni equilibrium phases produced by reduction of nanocrystalline NiFe2O4. *Solid State Commun.* **128**, 345 (2003).
22. Goto, S. et al. Synthesis of single-phase L10-FeNi magnet powder by nitrogen insertion and topotactic extraction. *Sci. Rep.* **7**, 13216 (2017).
23. Hlova, I. Z. et al. Enhancement of hard magnetism and chemical order of synthetic $L1_0$-FeNi. *J. Alloys Compd.* **981**, 173619 (2024).
24. Meneses, F. et al. $L1_0$-FeNi ordered phase in AC electrodeposited iron-nickel biphasic nanowires. *J. Alloys Compd.* **766**, 373 (2018).
25. Ke, J.-H., Young, G. A. & Tucker, J. D. Ab initio study of phosphorus effect on vacancy-mediated process in nickel alloys – An insight into Ni2Cr ordering. *Acta Mater.* **172**, 30–43 (2019).
26. Hernando, A. & Kulik, T. Exchange interactions through amorphous paramagnetic layers in ferromagnetic nanocrystals. *Phys. Rev. B* **49**(10), 7064 (1994).
27. Popov, A. G. & A, V. Korolyov and V. S. Gaviko,. Abnormal temperature dependence of coercivity of Sm–Co–Fe–Cu–Zr alloys: history and current state. *J. Magn. Magn. Mater.* **272**, E1883–E1885 (2004).
28. Karube, K. et al. Doping control of magnetic anisotropy for stable antiskyrmion formation in schreibersite (Fe,Ni)3P with $_S4$ symmetry. *Adv. Mater.* **34**, 2108770 (2022).
29. P. Villars and K. Cenzual, "Pearson's Crystal Data: Crystal Structure Database for Inorganic Compounds," ed. Materials Park: ASM International, 2021.
30. Pecharsky, V. K. & Zavalij, P. Y. *Fundamentals of Powder Diffraction and Structural Characterization of Materials* (Springer, 2005).
31. D. Balzar *et al.*, "Size–strain line-broadening analysis of the ceria round-robin sample," *urn:issn:0021–8898,* **37** (6): (2004).
32. O'Handley, R. C. *Modern Magnetic Materials: Principles and Applications* (Wiley, 1999).

Acknowledgements

We thank Manuel Vazquez for useful discussions and Lindsay Greer for illuminating discussions and for communicating results prior to publication.

Author contributions

A. Hernando: Conceptualization, Supervision, Writing; P. de la Presa, D. Arranz-López, M.P. Marín: Data SQUID, Analysis; J. A. Jimenez-Rodriguez and A. García-Escorial: Data electron microscopy, Analysis; J. Calvo: sample fabrication; I. Llamas, C. Navío: Discussion and validation of data; R. Miranda: Funding, Supervision, Writing and Editing.

Funding

The research was financially supported by the "Severo Ochoa" Programme for Centres of Excellence in R&D (CEX2020-001039-S), by the Regional Government of Madrid through NANOMAGCOST project (S2018/NMT-4321) and by the Spanish Ministry of Science through the projects PID2021-123112OB-C21, PDC2022-133039-I00 and TED2021-129688B-C21.

Declarations

Competing interests

The authors declare no competing interests.

Additional information

Supplementary Information The online version contains supplementary material available at https://doi.org/10.1038/s41598-026-36990-5.

Correspondence and requests for materials should be addressed to R.M.